Nodeless Variable Finite Elements with Flux-Based Formulation for Heat Transfer Analysis

Sutthisak Phongthanapanich[1], Suthee Traivivatana[2], and Pramote Dechaumphai[3*]

[1] Department of Mechanical Engineering, Siam University, 235 Petchkasem Road, Phasi-charoen, Bangkok 10163, Thailand,
Tel: 0-2457-0068, E-mail: sutthisakp@yahoo.com

[2,3] Department of Mechanical Engineering, Chulalongkorn University, 254 Phyathai Road, Patumwan, Bangkok 10330, Thailand,
Tel: 0-2218-6621, Fax: 0-2218-6621 *E-mail: fmepdc@eng.chula.ac.th

Abstract

A nodeless variable element method is combined with the flux-based formulation to analyze two-dimensional steady-state and transient heat transfer problems. The nodeless variable element employs quadratic interpolation functions to provide higher solution accuracy without requiring additional actual nodes. The flux-based formulation is applied to reduce the complexity in deriving the finite element equations as compared to the conventional finite element method. The solution accuracy is further improved by implementing an adaptive meshing technique to generate finite element mesh that can adapt and move along with the solution behavior. The effectiveness of the combined procedure is evaluated by heat transfer problems that have exact solutions.

Keywords: Flux-based formulation, Finite element method, Heat transfer

1. Introduction

The finite element method has been widely used to solve for the response of aerospace structures caused by the thermal effect in the past decades [1]. New formulations have been developed and evaluated in order to improve the analysis solution accuracy, as well as to reduce the computational time [2,3]. For hypersonic vehicles design, intense aerodynamic heating may produce severe thermal stresses that can reduce the structural performance and may cause structural failure. Since the thermal stresses are sensitive to the thermal gradients, a thorough thermal analysis is required to predict detailed temperature distribution in order to produce accurate thermal stress solution. In the prediction of the temperature distribution, the conventional finite element formulation with standard finite element types is frequently employed. The solution accuracy is improved by simply refining the finite element model using consecutively smaller elements until a required convergence is met. The solution accuracy can also be improved by using the *h*-method of adaptation where the mesh is globally or locally refined or coarsened [2,4], or the *p*-method by increasing or decreasing the order of the element interpolation functions [5]. Recently, many researchers have proposed improved versions of the *r*-refinement method with moving mesh, so that mesh points are moved throughout the domain while the connectivity of the mesh is kept fixed [6].

The objective of this paper is to develop a procedure to improve the predicted temperature distribution by using an alternative finite element method. The nodeless variable finite element is introduced and employed in this paper in order to increase the temperature solution accuracy. The nodeless variable finite element uses quadratic interpolation functions to describe the temperature distribution over the element without requiring additional actual nodes. The use of nodeless variable finite element can also be referred to as a hierarchical methodology, since the element reduces to the standard linear element when the nodeless variables are constrained to zero or eliminated. The paper also introduces and implements the flux-based formulation to derive the finite element matrices for such nodeless variable element. The flux-based formulation can simplify the finite element computational procedure as compared to the conventional finite element method.

To further improve the solution accuracy for both the steady-state and the transient heat transfer analyses, an adaptive unstructured meshing technique [4,7] is also incorporated. The technique was first designed for analyzing hyperbolic problems, and has been modified recently for solving both the elliptic as well as the parabolic problems. For time-dependent heat transfer problems, especially where the thermal loads (such as the heat source) have magnitudes which vary with time and move along the body of the structure, the mesh employed must adapt itself both in time and space (mesh movement) to accurately capture the transient temperature response. The effectiveness of the combined procedure is demonstrated by the steady-state heat conduction analysis of a plate subjected to a highly localized surface heating.

2. Finite Element Thermal Analysis

2.1 Governing Equations and Boundary Conditions

For heat transfer in the two-dimensional solid domain Ω bounded by the surface S as shown in Fig. 1, the temperature response is governed by the energy equation that can be written in the conservation form as,

$$\frac{\partial U}{\partial t}+\frac{\partial E}{\partial x}+\frac{\partial F}{\partial y}=Q \tag{1}$$

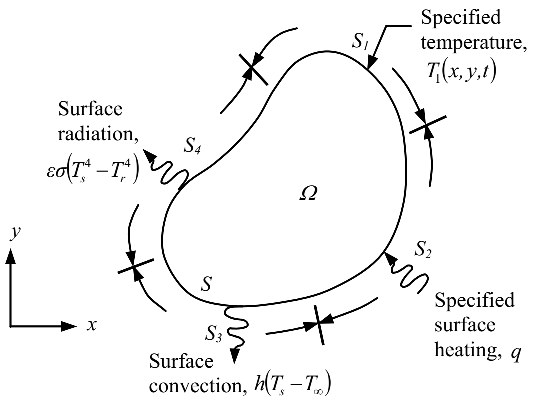

Figure 1. Domain and boundary conditions for two-dimensional heat transfer

where the conservation variable U and the heat flux components E and F are,

$$U=\rho cT \; ; \; E=q_x=-k\frac{\partial T}{\partial x} \; ; \; F=q_y=-k\frac{\partial T}{\partial y} \tag{2}$$

and Q is the heat source. The heat flux components q_x and q_y are related to the temperature gradients by Fourier's law. The energy equation shown in Eq. (1) is to be solved together with appropriate initial condition of,

$$T(x,y,0)=T_0(x,y) \tag{3}$$

and the boundary conditions which are the surface temperature T_s and the surface heat flux q_s that may consist of,

$$T_s=T_1(x,y,t) \qquad (\textit{specified temperature}) \tag{4a}$$

$$q_s=-q \qquad (\textit{specified surface heating}) \tag{4b}$$

$$q_s=h(T_s-T_\infty) \qquad (\textit{surface convection}) \tag{4c}$$

$$q_s=\varepsilon\sigma(T_s^4-T_r^4) \qquad (\textit{surface radiation}) \tag{4d}$$

where q_s is the conduction heat flux normal to the surface boundary, h is the convection coefficient, T_∞ is the medium temperature for convection, ε is the surface emissivity, σ is the Stefan-Boltzmann constant, and T_r is the medium temperature for radiation.

2.2 Nodeless Variable Flux-Based Finite Element Formulation

Finite element equations derived in this paper are based on the use of the Taylor-Galerkin algorithm [2]. The basic concept of the Taylor-Galerkin algorithm is to use the Taylor-series expansion in time to establish recurrence relations for time marching, and the method of weighted residuals with Galerkin's criterion for spatial discretization. The flux-based formulation [3] is implemented to derive the finite element equations for the nodeless variable element. For the triangular nodeless variable element, the distribution of temperature over the element is assumed in the form,

$$T(x,y,t)=\sum_{i=1}^{6}N_i(x,y)T_i(t)=\lfloor N(x,y)\rfloor\{T(t)\} \tag{5}$$

where $\lfloor N(x,y)\rfloor$ consists of the element interpolation functions and $\{T(t)\}$ is the vector of the unknown temperatures and the nodeless variables. The nodal temperatures are T_1 through T_3, while T_4 through T_6 are the nodeless variables. The element interpolation functions, N_1, N_2, N_3 are identical to the element interpolation functions L_1, L_2, L_3 used for the standard three-node triangular element. The nodeless variable interpolation functions implemented in this paper are,

$$N_4=L_2L_3 \; ; \; N_5=L_1L_3 \; ; \; N_6=L_1L_2 \tag{6}$$

Each nodeless variable interpolation function varies quadratically along one edge and vanishes along the other edges as highlighted by the example of N_6 in Fig. 2. To derive the finite element matrices using the flux-based formulation, the method of weighted residuals is first applied to Eq. (1),

$$\int_\Omega N_i\left(\frac{\partial U}{\partial t}+\frac{\partial E}{\partial x}+\frac{\partial F}{\partial y}-Q\right)d\Omega=0 \tag{7}$$

where Ω is the element domain. The Gauss's theorem is then applied to the flux derivative terms to yield,

$$\int_\Omega N_i\frac{\partial E}{\partial x}d\Omega=\int_S N_iEn_x d\Gamma-\int_\Omega\frac{\partial N_i}{\partial x}Ed\Omega \tag{8}$$

$$\int_\Omega N_i\frac{\partial F}{\partial y}d\Omega=\int_S N_iFn_y d\Gamma-\int_\Omega\frac{\partial N_i}{\partial y}Fd\Omega \tag{9}$$

where S is the element boundary. Then, the first-order forward differencing is used to approximate the time derivative term as,

$$\frac{\partial U^n}{\partial t}\cong\frac{U^{n+1}-U^n}{\Delta t}=\frac{\Delta U}{\Delta t} \tag{10}$$

Substituting Eqs. (8)-(10) into Eq. (7) to yield,

$$\begin{aligned}\int_\Omega N_i\frac{\Delta U}{\Delta t}d\Omega=&\int_\Omega\frac{\partial N_i}{\partial x}Ed\Omega+\int_\Omega\frac{\partial N_i}{\partial y}Fd\Omega\\&-\int_S N_iEn_x d\Gamma-\int_S N_iFn_y d\Gamma\\&+\int_\Omega N_iQd\Omega\end{aligned} \tag{11}$$

The unknown increments, ΔU, are also approximated in the form,

$$\Delta U=\sum_{i=1}^{6}N_i\Delta U_i=\lfloor N\rfloor\{\Delta U\} \tag{12}$$

where

$$\Delta U_i=\rho c(T_i^{n+1}-T_i^n) \tag{13}$$

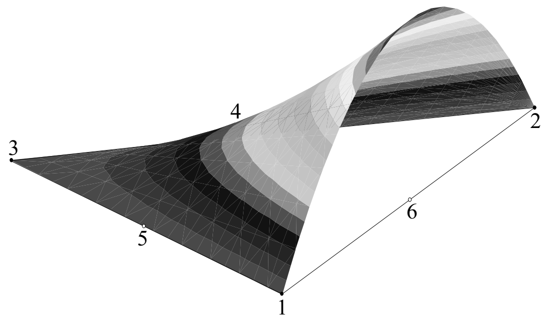

Figure 2. An example of N_6 interpolation function for a typical triangular element

In the above Eq. (13), the superscript n denotes the time step while the subscript i denotes the actual node and the nodeless variable. In the flux-based formulation, the element flux distributions are computed from the nodal fluxes as,

$$E = \sum_{i=1}^{3} \overline{N}_i E_i^n = \lfloor \overline{N} \rfloor \{E^n\}$$
$$F = \sum_{i=1}^{3} \overline{N}_i F_i^n = \lfloor \overline{N} \rfloor \{F^n\} \tag{14}$$

where $\lfloor \overline{N} \rfloor$ are the standard linear element interpolation functions, i.e., $\lfloor L_1 \quad L_2 \quad L_3 \rfloor$. The $\{E^n\}$ and $\{F^n\}$ are the vectors of the nodal heat fluxes that relate to the temperature gradients through Fouries's law which are given by,

$$\{E^n\} = \begin{Bmatrix} -k \left\lfloor \dfrac{\partial N}{\partial x} \right\rfloor \{T^n\} \Big|_1 \\ -k \left\lfloor \dfrac{\partial N}{\partial x} \right\rfloor \{T^n\} \Big|_2 \\ -k \left\lfloor \dfrac{\partial N}{\partial x} \right\rfloor \{T^n\} \Big|_3 \end{Bmatrix} \; ; \; \{F^n\} = \begin{Bmatrix} -k \left\lfloor \dfrac{\partial N}{\partial y} \right\rfloor \{T^n\} \Big|_1 \\ -k \left\lfloor \dfrac{\partial N}{\partial y} \right\rfloor \{T^n\} \Big|_2 \\ -k \left\lfloor \dfrac{\partial N}{\partial y} \right\rfloor \{T^n\} \Big|_3 \end{Bmatrix} \tag{15}$$

The above nodal fluxes depend on the nodal temperatures and need to update at every time step for the transient analysis. Substituting Eqs. (12) and (14) into Eq. (11), the finite element equations are,

$$[M]\{\Delta U\}^{n+1} = \Delta t \left([D_x]\{E\}^n + [D_y]\{F\}^n + \{R\}^n + \{B\}^n \right) \tag{16}$$

where Δt denotes the time step, $\{\Delta U\}^{n+1} = \{U\}^{n+1} - \{U\}^n$ represents the vector of the increments of the nodal temperatures and the nodeless variables at the time step n+1. The matrix $[M]$ on the left-hand-side of Eq.(16) is the mass matrix defined by,

$$[M] = \int_A \{N\} \lfloor N \rfloor \, dA \tag{17}$$

where A is the element domain of integration. The matrices $[D_x]$ and $[D_y]$ in Eq. (16) are,

$$[D_x] = \int_A \left\{ \frac{\partial N}{\partial x} \right\} \lfloor \overline{N} \rfloor \, dA$$
$$[D_y] = \int_A \left\{ \frac{\partial N}{\partial y} \right\} \lfloor \overline{N} \rfloor \, dA \tag{18}$$

The element nodal vector $\{R\}$ associated with the heat source Q is,

$$\{R\} = \int_A \{N\} Q \, dA \tag{19}$$

and the vector $\{B\}$ representing the boundary nodal vector is,

$$\{B\} = \int_S \{N\} \lfloor \overline{N} \rfloor dA \left(l\{E\} + m\{F\} \right)$$
$$= \int_S \{N\} \lfloor \overline{N} \rfloor dA \{q\} \tag{20}$$

where l and m are the components of a unit vector normal to the element boundary. The vector $\{q\}$ appearing in the above Eq. (20) may be replaced by different types of boundary conditions as shown in Eqs. (4b-4d). The interpolation functions in Eq. (20) needed for integration along the element side S are,

$$N_1 = 1 - \frac{x}{L} \; ; \; N_2 = \frac{x}{L} \; ; \; N_3 = \frac{x}{L}\left(1 - \frac{x}{L}\right) \tag{21}$$

where L is the length of element edge and x is the local coordinate along the edge starting from node 1 as shown in Fig. 3. The finite element equations, Eq. (16) are derived for all the elements prior to assembling to yield the system equations. Appropriate boundary conditions of the given problem are then applied. Finally, the system equations are iteratively solved for the nodal temperatures and the nodeless variables.

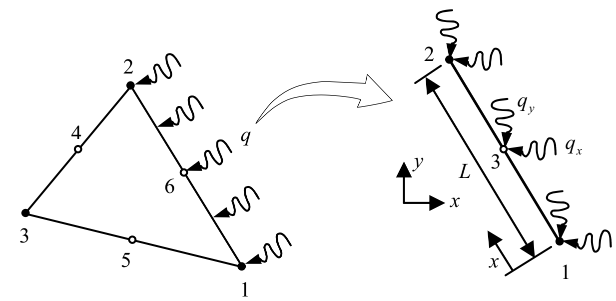

Figure 3. Discretization of heat flux into the actual nodes and the nodeless variable on a typical element edge

3. Adaptive Meshing Technique

There are two main steps in the implementation of the adaptive meshing technique, the first step is the determination of proper element sizes and the second step is the new mesh generation. The temperature T is used as the indicator for computing proper element sizes at different locations in the domain. As small elements must be placed in the region where changes in the temperature gradients are large, the second derivatives of the temperature at a point with respect to global coordinates x and y are needed. Using the concept of principal stresses determination from a given state of stresses at a point [2,7], the maximum principal quantities are then used to compute the proper element size h_i by requiring that the error should be uniform for all elements,

$$h_i^2 \lambda_i = h_{min}^2 \lambda_{max} = \text{constant} \tag{22}$$

where the subscript i, i = 1, 2, denotes the direction of the maximum and minimum element length, and λ_i is the higher principal quantity of the element considered,

$$\lambda_i = max\left(\left|\frac{\partial^2 T}{\partial X^2}\right|, \left|\frac{\partial^2 T}{\partial Y^2}\right|\right) \tag{23}$$

In Eq. (22), λ_{max} is the maximum principal quantity for all elements and h_{min} is the minimum element size specified by users. The node spacing h_i is scaled according to the maximum value of the second derivatives of the temperature. Such technique generates small elements in the regions with large change in the temperature gradients to increase the analysis solution accuracy. At the same time, larger elements are generated in the other regions where the temperature profile is nearly uniform to reduce the computational time and the computer memory [4,7].

It should also be noted that the finite element solutions are closely related to the quality of the element shapes. Babuska and Aziz [8] demonstrated that the solution accuracy obtained from a mesh with triangles degrade seriously as the element largest angle is allowed to approach 180°. The mesh adaptation technique [7] implemented in this paper assures to provide good quality of the element shapes for all the meshes generated. The Taylor series expansion is used to interpolate the nodal solutions, such the temperature, from a previous mesh to a new mesh. According to the quality criterion presented by Ruppert [9], the minimum angle (γ) for a triangle to assure good element aspect ratio is given by,

$$\left|\frac{1}{\sin\gamma}\right| \le \frac{d_{longest}}{d_{shortest}} \le \left|\frac{2}{\sin\gamma}\right| \tag{24}$$

where d denotes the distance. The value of γ equals to 60° is used in this paper to calculate the element aspect ratio for producing the near-equilateral triangles in the process of generating all adaptive finite element meshes.

4. Algorithm Evaluation

To evaluate the performance of the nodeless variable finite elements using the flux-based formulation with the implementation of the adaptive meshing technique, two heat transfer problems that have exact solutions are presented. These problems are: (1) a steady-state heat conduction in a square plate subjected to a highly localized surface heating, (2) a transient heat transfer in a long plate subjected to a moving heat source.

4.1 Steady-State Heat Conduction in a Square Plate Subjected to a Highly Localized Surface Heating

The first example is a steady-state conduction heat transfer in a square plate due to a highly localized surface heating. The plate temperature distribution, which is a solution to the Poisson's equation with the boundary conditions of zero temperature along the four edges, is shown in Fig. 4. The applied surface heating distribution is given by,

$$\frac{q}{kt} = 2y(1-y)\left[\tan^{-1}\beta - \frac{\alpha(1-2x)}{\sqrt{2}(1+\beta^2)} + \frac{\alpha^2\beta x(1-x)}{2(1+\beta^2)^2}\right] + 2x(1-x)\left[\tan^{-1}\beta - \frac{\alpha(1-2y)}{\sqrt{2}(1+\beta^2)} + \frac{\alpha^2\beta y(1-y)}{2(1+\beta^2)^2}\right] \tag{25}$$

where q is the applied surface heating, k is the plate thermal conductivity, t is the plate thickness, and $\beta = \alpha\left(\sqrt{2}(x+y) - 0.8\right)$. The exact solution for the temperature distribution is,

$$T(x,y) = x(1-x)y(1-y)\tan^{-1}\beta \tag{26}$$

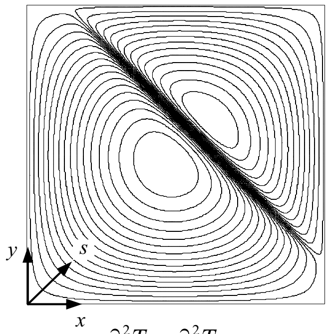

$$\frac{\partial^2 T}{\partial x^2} + \frac{\partial^2 T}{\partial y^2} = -\frac{q}{kt}$$

for $0 < x < 1$; $0 < y < 1$
with $T = 0$ along edges.

Figure 4. Governing differential equation, boundary conditions, and temperature contours for a unit square plate subjected to a highly localized surface heating

The temperature contours for the exact solution are shown in Fig. 4. The figure shows a steep temperature gradient along the s-direction at s equal to 0.8. The magnitude of the temperature gradient is caused by the large value of the parameter α which is selected as 100 in this paper. Both the temperature and the applied surface heating distributions along the plate diagonal in the s-direction are shown in Fig. 5. The figure shows the steep gradients and the rapid change of surface heating distribution in a narrow domain around s = 0.8.

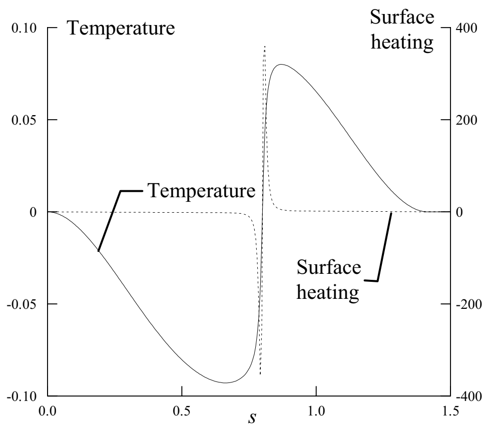

Figure 5. Plate temperature and surface heating distributions along a diagonal direction of the plate

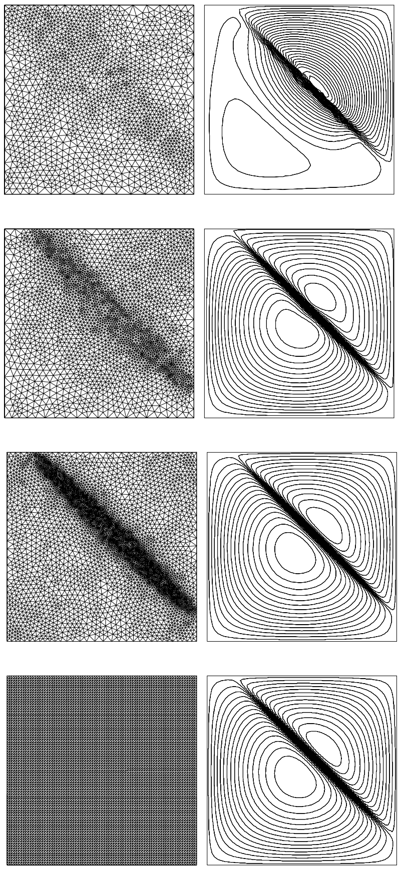

1st Mesh:
3,357 Triangles
1,721 Nodes
Quality = 99.26%

2nd Mesh:
5,959 Triangles
3,034 Nodes
Quality = 99.85%

3rd Mesh:
10,101 Triangles
5,121 Nodes
Quality = 99.92%

Uniform Mesh:
12,800 Triangles
6,561 Nodes

Figure 6. Uniform and adaptive meshes with their temperature solution contours for a plate subjected to a highly localized surface heating

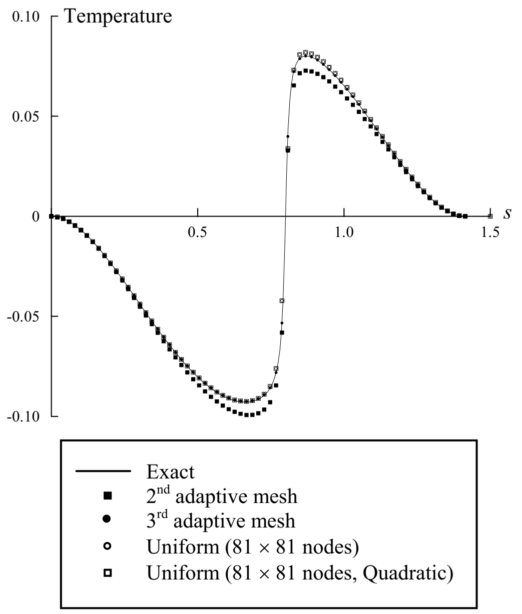

Figure 7. Comparison of the exact temperature solution and the predicted temperatures from the uniform and adaptive meshes

Both the adaptive meshes and a uniformly refined mesh are used in the analysis to evaluate the performance of the combined nodeless variable flux-based finite element method and the adaptive meshing technique. The nodeless variable finite element solutions on three adaptive meshes and the conventional finite element solution on a uniform refined mesh are shown in Fig. 6.

The figures show the solution improvement of the combined nodeless variable finite element method and the adaptive meshing technique as the mesh adapts itself automatically to the solution behavior. Figure 7 shows the comparison of the exact temperature and the predicted temperature solutions obtained from the nodeless variable finite element method using the adaptive meshes, and from the conventional finite element method using a uniform refined mesh. The figure shows that the third adaptive mesh solution with 10,101 nodeless variable finite elements agrees very well with the exact temperature solution. The figure also indicates that, in order to obtain the solution accuracy nearly at the same level as provided by the third adaptive mesh, a regular uniform mesh with at least 12,800 elements (81 × 81 nodes) is required.

4.2 Transient Conduction Heat Transfer in a Long Plate Subjected to a Moving Heat Source

To further evaluate the performance of the combined nodeless variable flux-based finite element method and the adaptive meshing technique, a transient conduction heat transfer in a long plate subjected to a moving heat source along an edge is considered. Figure 8 shows the problem statement of a steel plate, with the dimensions of 1" × 0.02", subjected to an intense moving heat source along the top edge. The heat source of 347.22 Btu/in^2 is simulated as a square pulse of 0.01" width that moves at a speed of 5 in/sec. With the boundary condition of 0^{o}F along the other three edges as indicated in the figure, the exact plate temperature response was derived in form of infinite series as given by Eq. (27) [10], where the origin and the directions of the $\xi - y$ coordinate system are shown in Fig. 8, q is the moving heat source, h is plate width, $H = \rho c v / 2k$, ρ is the plate density, c is the specific heat, v is the velocity of the moving heat source, and k is the plate thermal conductivity.

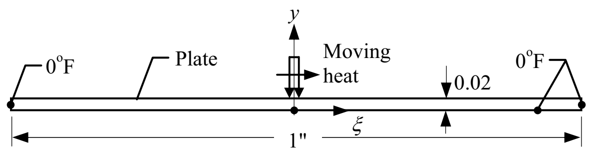

Figure 8. Problem statement for transient thermal analysis of a plate subjected to a moving heat source

$$T(\xi,y) = \frac{qe^{-H\xi}}{Lk}\{\sum_{n=2,4}^{\infty}\frac{1}{\lambda_n(H^2+\frac{n^2\pi^2}{4L^2})}[H(2\sin(\alpha)\cosh(HW)) - \frac{n\pi}{2L}(2\cos(\alpha)\sinh(HW))][\sin\left(\frac{n\pi\xi}{2L}\right)\frac{\sinh(\lambda_n y)}{\cosh(\lambda_n h)}] + \sum_{n=1,3}^{\infty}\frac{1}{\lambda_n(H^2+\frac{n^2\pi^2}{4L^2})}[H(2\cos(\alpha)\sinh(HW)) + \frac{n\pi}{2L}(2\sin(\alpha)\cosh(HW))][\cos\left(\frac{n\pi\xi}{2L}\right)\frac{\sinh(\lambda_n y)}{\cosh(\lambda_n h)}]\} \quad (27)$$

The parameter α and λ_n in Eq. (27) are defined by,

$$\alpha = \frac{n\pi w}{2L} \quad \text{and} \quad \lambda_n = \sqrt{\frac{n^2\pi^2}{4L^2} + H^2} \tag{28}$$

where L is the plate length, and w is the width of the moving heat source simulated by a square pulse.

To clearly evaluate the performance and compare the solution accuracy obtained from the conventional and the nodeless variable flux-based finite element methods, the steady-state heat transfer case of the problem is first used. For the steady-state condition when the heat pulse is at the center of the plate, the transient temperature solution as shown in Eq. (27) reduces to,

$$T_{steady} = \frac{8Lq}{\pi^2 k} \sum_{n=1,3}^{\infty} \frac{\sin(\alpha)\tanh(\frac{n\pi h}{2L})}{n^2} \tag{29}$$

Such steady-state solution behavior above represents a very high temperature with the magnitude of 581.82°F on the edge at the heat pulse impingement location. The high temperature is localized with very steep distribution in an approximate narrow band of 0.01".

Figure 9 shows sections of the four finite element models used for predicting the plate temperature response. The first three models are the structured mesh models with graded elements near the top edge. These three models are the crude, medium, and fine finite element models with 1,600, 6,400, and 25,600 standard triangular elements, respectively. The fourth model is an adaptive mesh model with 3,245 nodeless variable finite elements. The table in Fig. 9 compares the predicted peak temperature response at the heat pulse impingement location obtained from the different finite element mesh models using the conventional and the flux-based finite element methods. The values in the brackets denote the percentage error of the predicted peak temperature as compared to the exact solution. The table shows that the adaptive mesh uses fewer elements than the fine structured mesh but can provide higher solution accuracy. The table also indicates that the nodeless variable flux-based finite element method provides higher solution accuracy than the conventional finite element method for all the mesh models. Figure 10 shows the predicted temperature contours on the entire plate obtained from the nodeless variable finite element method.

For the case of transient heat transfer analysis, the combined adaptive meshing technique and the nodeless variable flux-based finite element method is used to predict the temperature response. The adaptive meshing technique is incorporated into the finite element method to adapt the mesh according to the transient solution behavior. Figure 11 shows the adaptive meshes and their temperature solution contours at three typical times. Detail of the adaptive mesh near the heat pulse impingement location and the temperature contours are shown in the lower figures. These figures show small clustered elements are generated in the region of high temperature gradients to capture the predicted peak temperature and the localized temperature distribution. At the same time, larger elements are generated in the other regions to reduce the computational time and the computer memory. Such a typical transient adaptive mesh consists of approximately 2,000 triangles. At the heat pulse impingement location, the predicted peak temperature is 572.62°F as compared to 573.07°F of the exact solution by Eq. (26) with the difference of less than 0.1%.

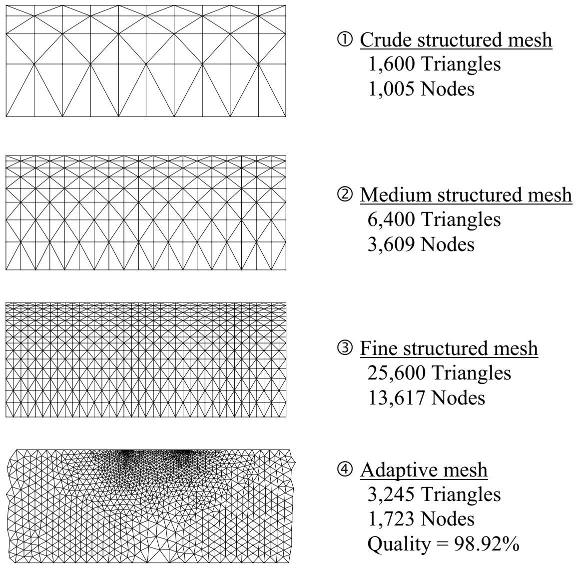

Mesh	Temperature (%Error) Conventional FE	Nodeless FE
①	558.40 (4.26)	583.23 (0.26)
②	575.83 (1.09)	581.86 (0.0073)
③	580.32 (0.27)	581.83 (0.0018)
④	581.36 (0.09)	581.82 (0.0000)

Figure 9. Comparison of the predicted peak temperatures obtained from the conventional and the nodeless variable finite element methods on both the graded structured and unstructured meshes

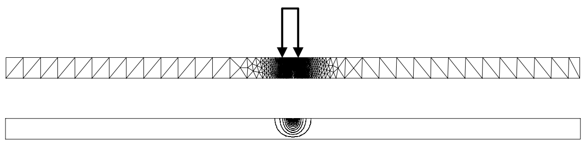

Figure 10. Adaptive mesh and temperature distribution contours for steady-state case

The comparison of the exact and the predicted temperature distributions along the top edge is shown in Fig. 12. The figure shows that the temperature distribution obtained from the combined adaptive meshing technique and the nodeless variable flux-based finite element method is in very good agreement with the exact solution.

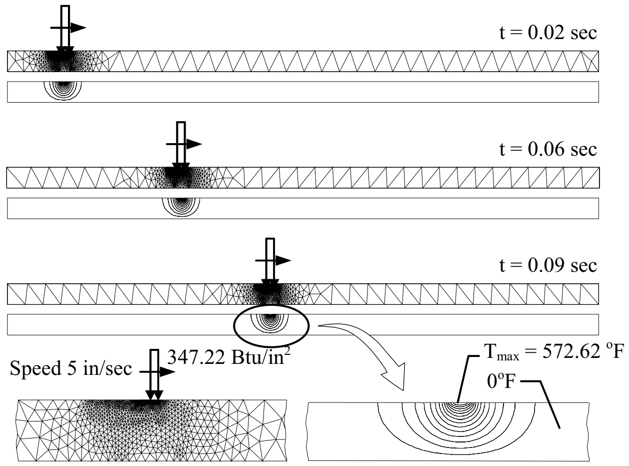

Figure 11. Adaptive mesh movement and the transient temperature response as the heat source moves across the plate

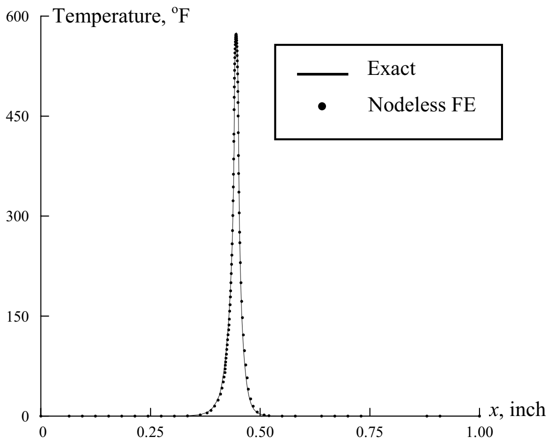

Figure 12. Comparison of the exact temperature solution and the predicted temperature distribution obtained from the combined adaptive meshing technique and the nodeless finite element method

5. Conclusion

The nodeless variable flux-based finite element method was developed to analyze two-dimensional steady-state and transient heat transfer problems. The nodeless variable finite element was described and their finite element equations were derived. The flux-based formulation was applied to reduce the computational complexity as compared to the conventional finite element method. The solution accuracy was further improved by implementing an adaptive meshing technique. The technique places small elements in the regions with large changes of temperature gradients. At the same time, larger elements are generated in other regions to reduce the total number of unknowns and the computational time. The combined procedure was evaluated by two heat transfer problems that have exact solutions. The problems are the steady-state heat conduction analysis of a plate subjected to a highly localized surface heating, and the transient thermal analysis of a plate subjected to a moving heat source. These problems show that the combined nodeless variable flux-based finite element method and the adaptive meshing technique can increase the analysis solution accuracy, and at the same time, reduce the total number of unknowns as compared to the standard nonadaptive mesh.

Acknowledgments

The authors are pleased to acknowledge the Thailand Research Fund for supporting this research work.

References

[1] Noor, A.K., 1999. Computational Structures Technology: Leap Frogging into the Twenty-First Century. Computers & Structures, Vol. 73, pp. 1-31.

[2] Dechaumphai, P., and Morgan, K., 1992. Transient Thermal-Structural Analysis using Adaptive Unstructured Remeshing and Mesh Movement. Thermal Structures and Materials for High-Speed Flight, AIAA, Washington, DC.

[3] Polesky, S.P., Dechaumphai, P., Glass, C.E., and Pandey, A.K., 1992. Three-Dimensional Thermal-Structural Analysis of a Swept Cowl Leading Edge Subjected to Skewed Shock-Shock Interference Heating. Journal of Thermophysics, Vol. 6, pp. 48-54.

[4] Phongthanapanich, S., and Dechaumphai, P., 2004. Mixed Entropy Fix Method for Roe's Flux-Difference Splitting Scheme with Automatic Mesh Generation. Transaction of CSME, Vol. 28, pp. 531-550.

[5] Zienkiewicz, O.C., and Taylor, R.L., 2000. Finite Element Method, volume 1: The basis, Fifth Edition. Woburn, Butterworth-Heinemann.

[6] Beckett, G., Mackenzie, J.A., and Robertson, M.L., 2001. A Moving Mesh Finite Element Method for the Solution of Two-Dimensional Stefan Problems. Journal of Computational Physics, Vol. 68, pp. 500-518.

[7] Phongthanapanich, S., and Dechaumphai, P., 2004. Two-Dimensional Adaptive Mesh Generation Algorithm and its Application with Higher-Order Compressible Flow Solver. KSME International Journal, Vol. 18, pp. 2190-2203.

[8] Babuska, I., and Aziz, A.K., 1976. On the Angle Condition in the Finite Element Method. SIAM Journal on Numerical Analysis, Vol. 13, No. 2, pp. 214-226.

[9] Ruppert J., 1995. A Delaunay Refinement Algorithm for Quality 2-Dimensional Mesh Generation. Journal of Algorithm, Vol. 18, No. 3, pp. 548-585.

[10] McGowan, D.M., Camarda, C.J., and Scotti, S.J., 1990. A Simplified Method of Thermal Analysis of a Cowl Leading Edge Subjected to Intense Localized Heating. NASA TP-16505.